MODELING OF SOUND TRANSMISSION THROUGH SHELL STRUCTURES WITH TURBULENT BOUNDARY LAYER EXCITATION

Yvette Y. Tang, Research Associate
National Research Council
MS 463, NASA Langley Research Center, Hampton, VA 23681

Richard J. Silcox, Assistant Branch Head
Jay H. Robinson, Research Engineer
Structural Acoustics Branch
MS 463, NASA Langley Research Center, Hampton, VA 23681

INTRODUCTION

The turbulent boundary layer (TBL) pressure field is an important source of cabin noise during cruise of high subsonic and supersonic commercial aircraft [1-3, 6]. The broadband character of this excitation field results in an interior noise spectrum that dominates the overall sound pressure level (SPL) and speech interference metrics in the forward and midcabins of many aircraft. In the authors' previous study [9], sound transmission through an aircraft fuselage, modeled by two concentric cylindrical sandwich shells and excited by a TBL statistical model was investigated analytically. An assessment of point and global structural vibration levels and resulting interior noise levels was obtained for different TBL models, flight conditions and fuselage structural designs. However, due to the complication of the shell structure, the important noise transmission mechanisms were difficult to discern. Previous experience has demonstrated that a fundamental understanding of the range of modes (or wavenumbers) generated by the TBL source both in the structure and the acoustic cavity is key to the development of both active and passive control technologies.

In an initial effort to provide this insight, the objective of this paper is to develop an analytical model of sound transmission through a simple unstiffened cylindrical aluminum shell excited by a TBL pressure field. The description of the turbulent pressure field is based on the Corcos formulation [2] for the cross-spectral density (CSD) of the pressure fluctuations. The coupled shell and interior and exterior acoustic equations are solved for the structural displacement and the interior acoustic response using a Galerkin approach to obtain analytical solutions. Specifically, this study compares the real part of the normalized CSD of the TBL excitation field, the structural displacement and the interior acoustic field. Further the modal compositions of the structural and cavity response are examined and some inference of the dominant mechanism of noise transmission is made.

MATHEMATICAL MODEL

A schematic of the system configuration considered is shown in Fig. 1, a finite cylindrical shell having hard end caps with radius R, length L, and wall thickness h immersed in fluid media. The mass density and sound speed are denoted as ρ_1 and c_1 and ρ_2 and c_2 for the external and internal fluids, respectively. Turbulent boundary layer pressure fluctuations convected by the flow in the external fluid along the streamwise direction excite the surface of the shell. A detailed analysis of the pressure fluctuations models has been presented in the references [2, 3, 6] and will not be repeated here. We shall instead, simply quote an expression for the spatial-frequency CSD of the pressure fluctuations S_p as following,

$$S_p(\xi, \eta, \omega) = \Phi(\omega)\, A(\xi,\omega)\, B(\eta,\omega)\, e^{i\omega\xi/U_c} \qquad (1)$$

where i = $\sqrt{-1}$, ω the frequency, $\xi = x_1 - x_2$ the streamwise separation along the longitudinal x direction and $\eta = R(\theta_1 - \theta_2)$ the crossflow separation along the circumferential θ direction, U_c the convective velocity of the flow, and Φ the power spectrum. Quantities A and B are exponential decaying functions along ξ and η.

Taking a Fourier transform of a Helmholz equations for the external and internal fluids and Donnell-Mushtari shell equation yields,

$$(\nabla^2 + \mathrm{i}\omega\beta_1 + k_1^2)\, p_1 = 0\,, \quad (\nabla^2 + \mathrm{i}\omega\beta_2 + k_2^2)\, p_2 = 0 \tag{2}$$

$$\widehat{L}(\omega)[w] = p_1 - p_2 - p \tag{3}$$

where $\nabla^2 = \partial(r\,\partial/\partial r)\partial r + (\partial^2/\partial\theta^2)/r^2 + \partial^2/\partial x^2$ in which r represents the radial cylindrical coordinate; $k_1 = \omega/c_1$ and $k_2 = \omega/c_2$ are wave numbers, β_1 and β_2 acoustic damping, and, p_1 and p_2 acoustic pressures of the external and internal fluids, respectively; p is the pressure generated by the TBL, $\widehat{L}$ is a differential operator whose explicit form can be found in text book [4], and w is the radial displacement component of the shell.

The flexible boundary conditions applied at both the outer and inner surfaces of the shell relate the pressures p_1 and p_2 to the shell displacement w

$$\left.\frac{\partial p_1}{\partial r}\right|_{r=R} = \rho_1\omega^2 w\,, \quad \left.\frac{\partial p_2}{\partial r}\right|_{r=R} = \rho_2\omega^2 w \tag{4}$$

A simply supported shell having hard end caps is represented by the following boundary conditions.

$$w = \frac{\partial^2 w}{\partial x^2} = 0\,, \quad \frac{\partial p_2}{\partial x} = 0\,, \quad \text{at } x = 0,\, L \tag{5}$$

Following the previous analysis [9], the displacement w is expanded in the orthogonal base functions X_{mn}

$$w = \sum_{m=1,\,n=0}^{\infty} w_{mn}\, X_{mn}(x,\theta) = \sum_{m=1,\,n=0}^{\infty} w_{mn} \sin(m\pi x/L)\cos(n\theta) \tag{6}$$

where the modal coefficients w_{mn} are unknown. Similarly, expand the turbulent pressure loading p as

$$p = \sum_{m=1,\,n=0}^{\infty} p_{mn}\, X_{mn}(x,\theta)\,, \quad p_{mn} = \frac{\varepsilon_n}{\pi L}\left[\int_0^L \int_0^{2\pi} p(x,\theta,\omega) X_{mn}(x,\theta)\, dx\, d\theta\right] \tag{7}$$

where ε_n are Neumann factors, $\varepsilon_n = 1$ for $n = 0$ and $\varepsilon_n = 2$ otherwise.

It is convenient to expand the pressure p_1 and p_2 which satisfy Eq. (2) as

$$p_1 = \sum_{m=1,\,n=0}^{\infty} p_{1mn}\, H_n^2(\sigma_{1m} r)\, X_{mn}\,, \quad p_2 = \sum_{m=1,\,n=0}^{\infty} p_{2mn}\, J_n(\sigma_{2m} r)\, X_{mn} \tag{8}$$

where H_n^2 is a Hankel function of the second kind and J_n is a Bessel function of the first kind of order n, respectively, $\sigma_{1m}^2 = k_1^2 - (m\pi/L)^2 - \mathrm{i}\omega\beta_1$ and $\sigma_{2m}^2 = k_2^2 - (m\pi/L)^2 - \mathrm{i}\omega\beta_2$, and p_{1mn} and p_{2mn} are unknown modal coefficients.

Substituting Eqs. (6) to (8) into (2) through (4) and then solving these coupled equations simultaneously for w_{mn}, p_{1mn}, p_{2mn} yield,

$$\{w_{mn},\, p_{1mn},\, p_{2mn}\} = \{H_{wmn},\, H_{p1mn},\, H_{p2mn}\}\, p_{mn} \tag{9}$$

where

$$\{H_{wmn},\, H_{p1mn},\, H_{p2mn}\} = \{1/(\mathrm{i}\,\omega),\, -Z_{mn}^J/J_{mn},\, -Z_{mn}^H/H_{mn}\}/(Z_{mn}^S + Z_{mn}^H - Z_{mn}^J) \tag{10}$$

$$Z_{mn}^H = \mathrm{i}\rho_1\,\omega H_{mn}^{2'}/(\sigma_{1m} H_{mn}^2), \quad Z_{mn}^J = \mathrm{i}\rho_2\,\omega J_{mn}'/(\sigma_{2m} J_{mn}) \tag{11}$$

The primes in above equation denote derivative with respect to the argument and Z_{mn}^S is the shell modal impedance.

The cross-spectral density for the wall displacement response and interior pressure takes the form

$$S_w = \sum_{m=1,\,n=0}^{\infty} |H_{wmn}|^2 \sin(m\pi x_1/L)\sin(m\pi x_2/L)\cos(n\theta_1)\cos(n\theta_2) S_{p_{mn}} \tag{12}$$

$$S_{p_2} = \sum_{m=1,\,n=0}^{\infty} |\widehat{H}_{p2mn}|^2 |J_n(\sigma_{2m} r_1)\, J_n^*(\sigma_{2m} r_2)\cos(m\pi x_1/L)\cos(m\pi x_2/L)\cos(n\theta_1)\cos(n\theta_2) S_{p_{mn}} \tag{13}$$

where * denotes the complex conjugate, $0 \le r_1, r_2 \le R$, $0 \le x_1, x_2 \le L$, $-\pi \le \theta_1, \theta_2 \le \pi$, and the modal spectral density of the generalized forces $S_{p_{mn}}$ is defined by

$$S_{p_{mn}} = \mathrm{Re}\,|\,4\Phi(\omega)\,\varepsilon_n\,(\pi L R_1)^{-1}\,(\alpha'\beta)^{-1}|\times[1-(-1)^n e^{-\beta R_1 \pi}]\times\{1+[n/(\beta R_1)]^2\}^{-1}\times \{1+[m\pi/(\alpha' L)]^2+2[1-(-1)^m e^{-\alpha' L}]\times(m\pi)^2(\alpha' L)^{-3}\}\times\{1+[m\pi/(\alpha' L)]^2\}^{-2} \quad (14)$$

In Corcos model, $\alpha' = (0.11+\mathrm{i})\omega/U_c$ and $\beta = 0.77\omega/U_c$.

It should be pointed out that the modal basis function for the pressure p_2, Eq. (8), does not satisfy the force boundary conditions in Eq. (5). Therefore, it is necessary to expand the orthogonal base functions X_{mn} in terms of $\cos(m\pi x/L)\cos(n\theta)$. The result gives the modal coefficient $\widehat{H}_{p2mn}$ as following

$$\widehat{H}_{p2mn} = \sum_{j=0,\, j\neq m}^{\infty} \frac{\varepsilon_n\, m\,[1-(-1)^{m-j}]}{\pi\,(m^2-j^2)}\, H_{p2jn} \quad (15)$$

Since both the excitation and cylindrical shell are symmetric in θ, integration of Eqs. (12) and (13) yields the average CSD

$$\{\overline{S}_w, \overline{S}_{p2}\} = \sum_{m=1,\, n=0}^{\infty} \{\overline{S}_{w_{mn}}, \overline{S}_{p2mn}\} = \sum_{m=1,\, n=0}^{\infty} \{|H_{wmn}|^2, |H_{p2mn}|^2\} S_{p_{mn}}/2 \quad (16)$$

Summation of the components either m or n in above equation yields the modal CSD

$$\{\overline{S}_{w_m}, \overline{S}_{p2m}\} = \sum_{n=0}^{\infty} \{\overline{S}_{w_{mn}}, \overline{S}_{p2mn}\}\,, \quad \{\overline{S}_{w_n}, \overline{S}_{p2n}\} = \sum_{m=1}^{\infty} \{\overline{S}_{w_{mn}}, \overline{S}_{p2mn}\} \quad (17)$$

RESULT AND DISCUSSION

The geometry and material properties of the shell chosen herein are taken from reference [5] for this study. The aluminum shell has the overall dimensions of R = 0.83m, L = 3.65m, and h = 0.0017m. Young's modulus and Poisson's ratio are E = 72GPa and μ = 0.3, respectively and the mass density is ρ = 2740kg/m^3. A structural loss factor is modeled as a small imaginary part of both Young's modulus $E(1+\mathrm{i}0.05)$ and a corresponding shear modulus. The value of acoustic damping is chosen as 0.005 providing representative damping levels. It is assumed that the aircraft is in flight at 35,000ft altitude (ρ_1 = 0.3795kg/m^2, c_1 = 296.556m/s) and is pressurized at 10,000ft (ρ_2 = 0.9041kg/m^3, c_2 = 328.558m/s). The free stream velocity of the turbulent flow is taken from Maestrello [6] for U_∞ = 425.48m/s and then the convection velocity is defined by $U_c = 0.8U_\infty$.

The result presented in the following will be two parts: Part one will address the coherence functions of the two-point spatial correlation of the excitation, shell response (displacement), and the cavity response (pressure). It is pointed out [8] that the modal spectra for the shell and cavity responses are more useful from the viewpoint of developing noise control systems than the highly detailed physical variables. Therefore, part two will examine the modal response of the cross-spectral density for both the shell and acoustic cavity responses. A dominant (or highly excited) mode is indicated by a dark square. The values in all the following plots are normalized by its own maximum and only the real part is considered.

Figures 2 and 3 show the CSD of the excitation (TBL pressure fluctuations, S_p) and the corresponding shell and acoustic responses (S_w and S_{p2}) versus the spatial separation in the streamwise ξ/L and cross-streamwise $\eta/(2\pi R)$ for ω = 300Hz and 2500 Hz, respectively. The reference coordinate is selected as $x_2 = 0.48L$ to avoid the nodes at which some modes can not be excited. Therefore, a slightly asymmetric behavior is shown in Fig. 2. Since the excitation is independent of the circumferential coordinate selected, the reference coordinate is $\theta_2 = 0$. Inspection of Fig. 2 reveals that the envelope of the shell response decays with an increase of the spatial separation, in a similar manner as does the excitation. The rate of decrease depends on the frequency of the forcing function. The results illustrate that the shell response at two widely separated points is generally correlated at low frequency ω = 300Hz and is uncorrelated at high frequency ω = 2500Hz. However, for the acoustic response, we do not observe a similar decaying relationship as for the shell response. The new feature can be explained by the following: When the TBL pressure fluctuations excite the shell at a particular frequency, many shell modes are excited as resonant modes. However, only some of these shell resonant modes are efficiently coupled to those cavity modes near resonance. Therefore, the dissipation of the acoustic CSD along the spatial separation can not be seen when an insufficient number of cavity modes are excited. If the shell

radius is increased (actually increasing the excited cavity modes), a stronger decay of the CSD is observed.

Figure 4 shows the modal cross-spectral density of the shell response $\bar{S}_{w_n}$ and the acoustic response $\bar{S}_{p2n}$ versus the circumferential mode n and frequency ω. High mode levels occur in the shell response in a line between $13 \le n \le 22$ over the range of frequencies plotted, as shown in Fig. 4(a). A strong filtering effect is observed in comparing the cavity mode response and the shell wavenumber mode response. Most low order acoustic cavity modes between $1 \le n \le 7$ are strongly excited, but most of the high order circumference modes are reduced in the cavity response.

Figures 5 and 6 display the modal cross-spectral density of the shell and acoustic responses $\bar{S}_{wmn}$ and $\bar{S}_{p2mn}$ for ω = 100Hz and 300Hz, respectively. There is strong shell response over a range of resonant shell modes and this range expands to higher order modes with an increase of frequency. This demonstrates that with increasing frequency, an expanded locus of resonant modes is responding. For the acoustic response, these resonant shell modes drive a forced response of the corresponding acoustic modes and in addition excite some low order cavity modes into resonance. Similar behavior was observed for the modal structural and acoustic response from point force excitation [8]. This shows that the CSD of the cavity response is not only characterized by the "forced" modes generated by the shell vibration, but also by the cavity modes, especially for high frequency.

CONCLUSION

In this paper, an analytical model for prediction of the CSD of both the shell and acoustic responses of a finite cylindrical shell due to TBL excitation based on the Corcos TBL model was developed. The real part of the normalized CSD at two-points versus a spatial separation of the forcing field and response fields are calculated and presented. Modal behavior is examined in the low frequency range (100 Hz to 300Hz). The following conclusions can be drawn:

The CSD of the shell response are generally correlated at low frequency and the envelope of the correlation function decays with an increase of the spatial separation. The decay occurs much more rapidly at higher frequencies. However, the correlation function of the CSD of the cavity response does not decay with an increase of the spatial separation and frequency. With wavenumber filtering, highly excited cavity modes are reduced in number compared with the shell modes. Most of the cavity mode response is forced by the shell modes. However, some low order cavity resonant modes are excited.

REFERENCE

1. *Mechanics of flow-induced sound and vibration*, William K. Blake, (Vol. I and II, Academic Press, Inc., 1986)
2. "Resolution of pressure in turbulence", G. M. Corcos, *J. Acoust. Soc. Am.*, **35**(2), 192-199 (1963)
3. "Characteristics of the field of turbulent wall pressure fluctuations at large Reynolds numbers", B. M. Efimtsov, *Sov. Phys. Acoust.*, **28**(4), 289-292 (1982)
4. *Vibration of shells*, A. W. Leissa, 245-269 (NASA SP-288, 1973)
5. "Piezoelectric actuator models for active sound vibration control of cylinders", Harold C. Lester and S. Lefebvre, J. Int. Mat. Sys and Struct., **4**, 295-306 (1993)
6. "Radiation from and panel response to a supersonic turbulent boundary", L. Maestrello, *J. Sound. Vib.*, **10**(2), 261-295 (1969)
7. "Flow excitation of cylindrical shells and associated coincidence effects", J. V. Rattayya and M. G. Junger, *J. Acoust. Soc. Am.*, **36**(5), 878-884 (1964)
8. "Propeller modeling effects on interior noise in cylindrical cavities with application to active control", R. J. Silcox and H. Lester, AIAA 12th Aeroacoustic Conference, April 10-12, San Antonio, TX, Paper No. 89-1123 (1989)
9. "Sound transmission through cylindrical shell structures excited by boundary layer pressure fluctuations", Y. Y. Tang, R. J. Silcox, and J. H. Robinson, The 2nd AIAA/CEAS Aeroacoustics Conference, May 6-8, State College, PA, Paper No. 96-1760 (1996)

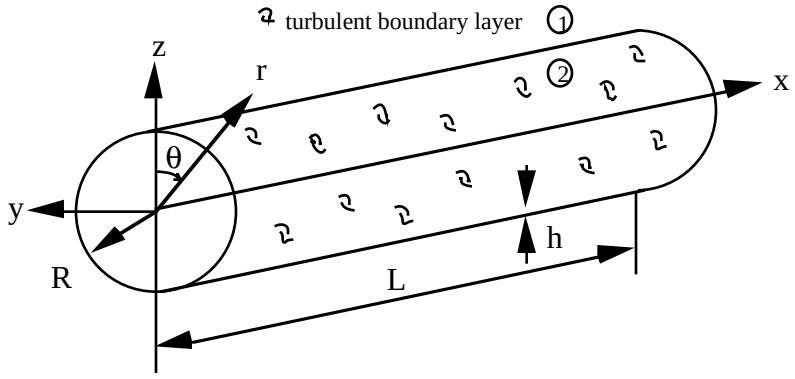

Figure 1. Schematic of system configuration.

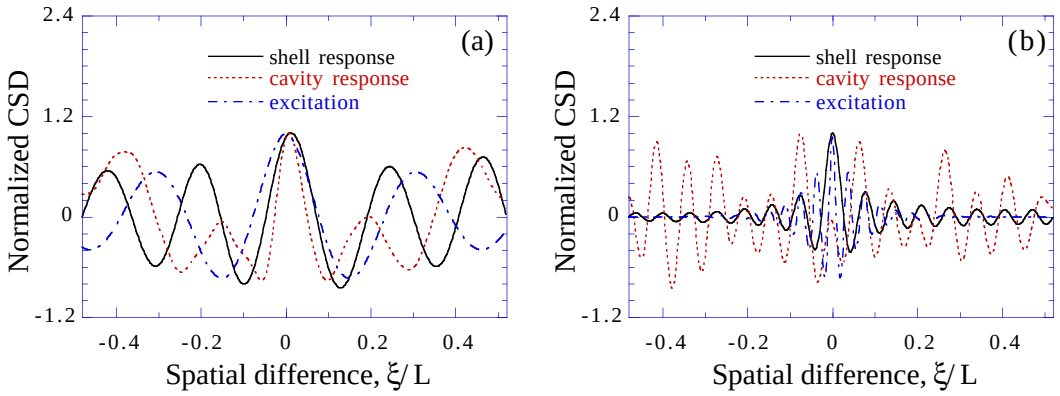

Figure 2. The normalized cross-spectral density versus the spatial differences ξ/L in the streamwise direction: (a) $\omega = 300$Hz; (b) $\omega = 2500$Hz.

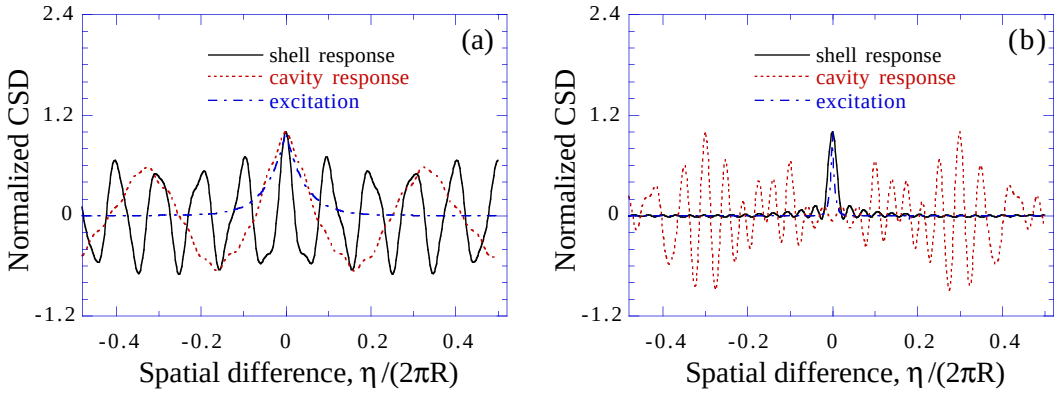

Figure 3. The normalized cross-spectral density versus the spatial differences ξ/L in the cross-streamwise direction: (a) $\omega = 300$Hz; (b) $\omega = 2500$Hz.

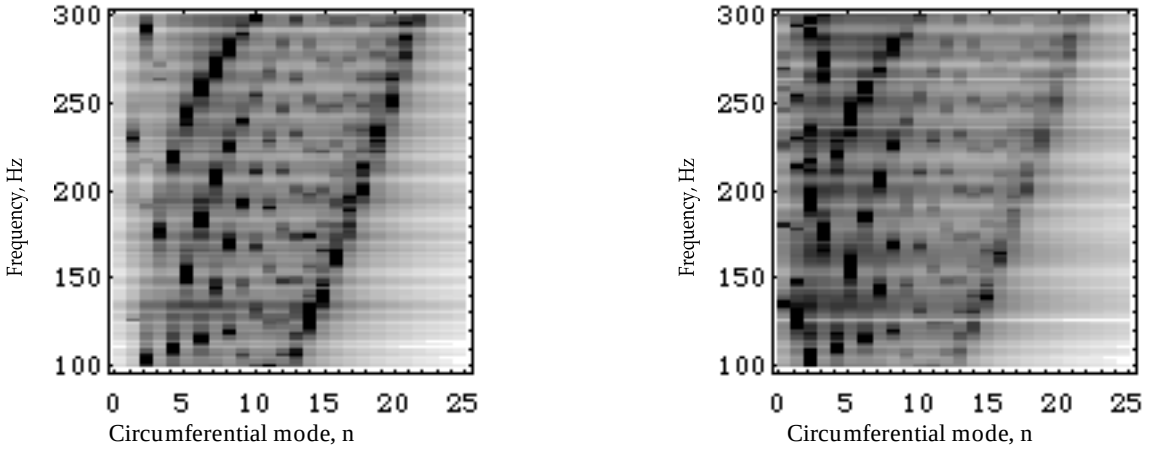

Figure 4. Modal cross-spectral density versus circumferential mode and frequency: varying from 0 to -30dB. (a) shell response $\overline{S}_{w_n}$; (b) cavity response $\overline{S}_{p_{2n}}$.

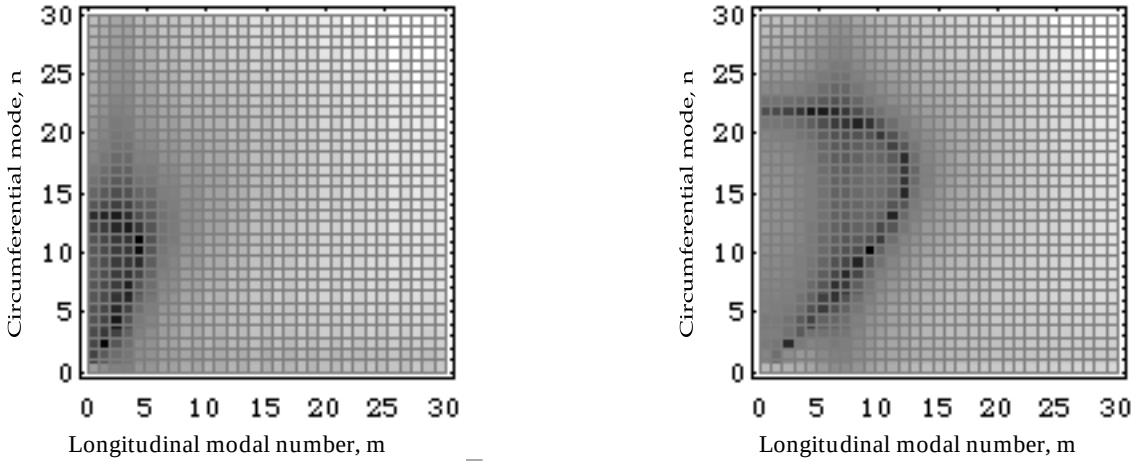

Figure 5. Modal cross-spectral density $\overline{S}_{w_{mn}}$ versus longitudinal and circumferential modes m and n: varying from 0 to -30dB. (a) ω = 100Hz; (b) ω = 300Hz.

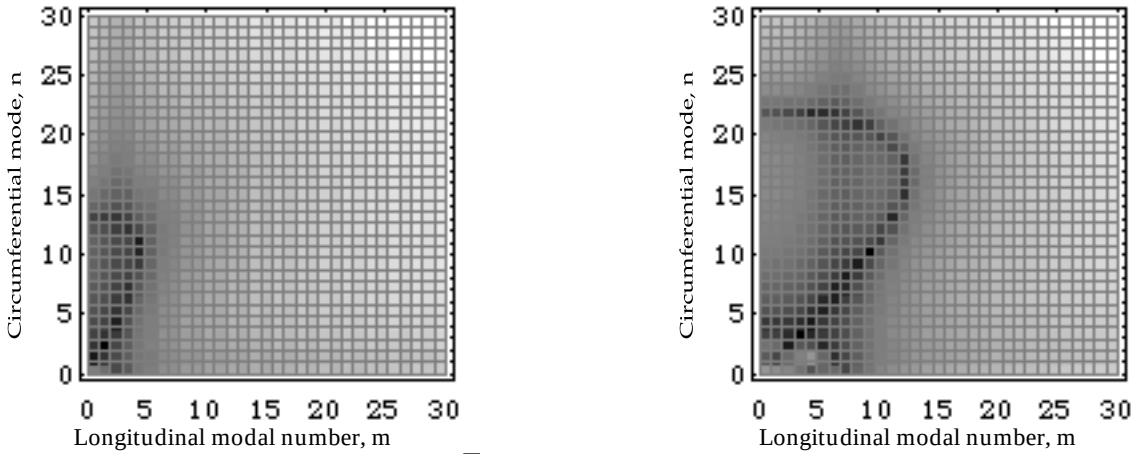

Figure 6. Modal cross-spectral density $\overline{S}_{p_{2mn}}$ versus longitudinal and circumferential modes m and n: varying from 0 to -30dB. (a) ω = 100Hz; (b) ω = 300Hz.